Nevenka R. Elezović[1], Mila N. Krstajić Pajić[2],*
Vladimir D. Jović[1]

[1]*University of Belgrade, Institute for Multidisciplinary Research,*
  Belgrade, Serbia,

[2]*University of Belgrade, Faculty of Technology and Metallurgy,*
  Belgrade, Serbia

Sub-monolayers of iridium electrodeposited on Ti₂AlC substrate as catalysts for hydrogen evolution reaction in sulfuric acid solution

ABSTRACT

The hydrogen evolution reaction (HER) was investigated at sub-monolayers of iridium electrodeposited on Ti₂AlC substrate. The lowest amount of electrodeposited iridium was 3 close-packed (111) monolayers (3 ML), while the highest one was 22 ML (3, 5, 10, 15 and 22 ML). The lowest and the highest amounts of iridium were electrodeposited by linear sweep voltammetry (LSV), while the other three samples were electrodeposited by controlled potential coulometry, from the solution containing 1 mM, or 3 mM K_3IrCl_6 + 0.5 M Na_2SO_4 (pH 6.2) at 70 °C. The HER was investigated by polarization and electrochemical impedance spectroscopy (EIS) measurements. Polarization curves for iridium sub-monolayers equal, or higher than 6 ML showed low Tafel slope of -14 to -16 mV dec^{-1} up to about -0.1 A cm^{-2}, while at higher current densities the Tafel slopes increased, varying between -40 and -72 mV dec^{-1}. The highest value of exchange current density (j_o) was obtained for 6 ML of electrodeposited iridium, being -27.89 A g^{-1}. The overpotential at j = -0.3 A cm^{-2} could be determined for samples containing 15 ML and 22 ML of iridium, being 82 mV.

Keywords: *Sub-monolayer, iridium electrodeposition, hydrogen evolution, sulfuric acid*

1. INTRODUCTION

1.1. The HER on iridium in acid solutions

Although it has been reported that the experimental reaction rate of HER in alkaline solutions is much slower than that in acid solutions [1], the development of efficient electrocatalysts for the HER in acid media is of great importance for polymer electrolyte membrane (PEM) electrolyzers, but the corrosion of non-noble metal substrates in acids is still a great problem.

According to the literature [2-8], the iridium oxide electrodes were considered as the most efficient oxygen evolution reaction (OER) electrocatalysts in acid media. Unfortunately, there are only few reports on iridium based catalysts for the HER in acid media [9,10].

Bimetallic iridium based nanostructures, characterized by high specific surface area and strong binding energy between nanoclusters and support were reported by Pi et al. [11] as highly efficient in acidic water electrolysis.

These nanocatalysts exhibited excellent activity and durability for oxygen evolution as well as for hydrogen evolution reaction. Bimetallic iridium-nickel was reported as the best performance one [11].

Highly active iridium nanocrystalline catalysts were synthesized by applying etching of multimetallic solid nanocrystals using Fe^{3+} ions and tested as the catalysts for water splitting [12]. The Ir-Co nanocatalysts exhibited the best performance for hydrogen evolution reaction, with 35 mV overpotential at the current density of 20 mA cm^{-2}, even comparable to the commercially available Pt/C [12].

Iridium-nickel-iron nanoparticles with homogeneous particle size distribution, synthesized by colloidal synthesis procedure, exhibited high activity and durability for both, anodic and cathodic reactions in water electrolysis - the overpotential for the HER in 0.5 M $HClO_4$ was 24 mV at the current density of 10 mA cm^{-2} [13]. It was explained by strong synergistic electronic effect between Ir, Ni and Fe [13].

Ir nanoparticles supported by 3D graphite foam was reported as a novel bifunctional catalyst for efficient water splitting in acid electrolyte [14]. This nanostructured catalyst showed excellent electrocatalytic activities for the HER, as well as for the OER [14].

*Corresponding author: Nevenka R. Elezović

E-mail: nelezovic@tmf.bg.ac.rs

Iridium-cobalt alloy based nanostructured catalysts exhibited excellent HER activity in acid electrolyte [15] owing to the strong electronic interaction and alloying effect of Ir and Co at the atomic level [15].

Mahmood et al. [16] referred Ir nanoparticles spread over 3D organic network support as efficient catalysts for the HER. The activity of this electrocatalyst was exceptional - only 13.5 mV overpotential value at the current density of 10 mA cm^{-2} in 0.5 M H_2SO_4 [16].

Wet-chemical approach procedure was applied for synthesis of Iridium based nanowires with specific morphology and large electrochemically active surface area, that exhibited excellent catalytic activity for the HER in acidic media, if compared to the state-of-the-art carbon supported Pt nanocatalysts [17].

However, high price and low abundance in Earth core of Pt-group metals generally limits their use in water electrolysis. Namely, two strategies for minimization of noble metals loading and maximization of the active surface area to volume ratio were exploited in the literature: (a) alloying with non-noble metals, for instance applying atomic layer deposition [18], and (b) electrodeposition of very thin, low noble metal loading sub-monolayers [19,20].

1.2. Electrodeposition of iridium

The process of iridium electrodeposition has been the subject of several papers [21-25]. In most of these studies iridium was electrodeposited for corrosion protection purposes [22-24] from the Ir^{4+} salts as a consequence of the fact that Ir^{3+} d^6 complexes belong to the group of the most stable complexes, being extremely inert to ligand exchange [26]. The current efficiency for iridium electrodeposition was low (between 2 % and 45 %). High current efficiency (up to 100%) for electrodepositing thin (up to 20 nm) and porous iridium layers was reported in Ref. [25], proposing 4 steps in the overall process of adsorption-controlled reduction of $IrCl_6^{3-}$ to Ir^0, with the necessary steps being adsorption of $IrCl_6^{3-}$ ($IrCl_6^{3-}$ $_{(ads)}$) and adsorption of hydrogen ($H_{(ads)}$).

S.H. Ahn et al. [21] used a different approach to the process of Ir electrodeposition from the $IrCl_6^{3-}$ complex, based on the ligand exchange with the sulfate-based aqueous electrolyte. Although at the room temperature this exchange is very slow, after increasing solution temperature to 70 °C the exchange of ligands and stabilization of Ir^{3+} species [27,28] has been detected. Complexes such as $IrCl_{6-x}H_2O^{x-3}$ were formed and it was shown that

these complexes could be reduced to Ir^0. Well-defined cathodic peak corresponding to the iridium electrodeposition was detected on the cyclic voltammograms (CVs). At the potential of hydrogen evolution iridium electrodeposition was quenched, while during the reverse sweep this process again took place at potentials more positive than the potential of hydrogen evolution on the rotating Au disc electrode. The shape of the current density responses of the CVs during the electrodeposition of Ir on rotating Au electrode indicated that the reaction is dominated by the surface controlled processes, i.e. desorption of the anion adlayer, while formation of a complete monolayer of hydrogen terminates Ir electrodeposition process, contrary to the mechanism predicted by Ref. [25].

In our previous studies of the HER at Ru, Pd and Ir layers electrodeposited on Ti₂AlC substrate [29- 31] it was shown that Ti₂AlC substrate is completely stable in 0.5 M H_2SO_4 (no corrosion, nor the OER could be detected up to 2.244 V) and that thin layers of electrodeposited noble metals could be promising catalyst for the HER in acid solution. Hence, taking into account that Ti₂AlC support is well known as low cost, commercial product, in this work an attempt was made to electrodeposit sub-monolayers of iridium on Ti₂AlC support and investigate the HER in sulfuric acid solution on such electrodes.

2. EXPERIMENTAL

All solutions were prepared using 18.2 MΩcm^{-1} deionized water (Smart2PureUV, TKA) and p.a. chemicals (SIGMA-Aldrich). Both, electrodeposition and HER experiments, were performed by the potentiostat Refrence 600 (Gamry Instruments, Inc.).

2.1. Iridium electrodeposition

Iridium electrodeposition was carried out in a double-jacketed three-electrode cell, with Pt counter electrode and reference, saturated sulfate electrode (SSE), being placed in separate compartments. Counter and reference electrode compartments were held at the room temperature, while the main compartment was heated to the desired temperature. Counter electrode compart-ment, containing only supporting electrolyte, was connected to the main one by fritted junction, while the reference electrode (SSE) was placed in a side compartment connected to the main one through a bridge and a Luggin capillary, always containing only supporting electrolyte. All compartments were filled with 0.5 M Na_2SO_4 of the same pH, while necessary amount of K_3IrCl_6 was dissolved in the main compartment.

Working electrode was Ti$_2$AlC cylinder, the diameter d = 6 mm and thickness h = 2 mm, connected to the Pt wire on the back side using silver conducting epoxy paste and sealed in the epoxy resin, so that only front surface was exposed to the solution. The procedure of Ti$_2$AlC substrate preparation was explained in our previous papers [29-31]. Iridium was electrodeposited on Ti$_2$AlC substrate discs from the solution containing either 1 mM or 3 mM K$_3$IrCl$_6$ dissolved in a supporting electrolyte 0.5 M Na$_2$SO$_4$ of the pH 6.2. Five iridium electrodeposited sub-monolayers (3, 6, 10, 15 and 22 ML) were used for the investigation of the HER in 0.5 M H$_2$SO$_4$. Before the iridium electro-deposition, Ti$_2$AlC substrate discs were polished on emery papers 600, 1200, 2400 and 4000, and cleaned and reduced by hydrogen evolution in 0.5 M H$_2$SO$_4$ for 10 min at j = -0.1 A cm^{-2}.

2.2. HER investigations

HER was investigated in 0.5 M H$_2$SO$_4$ at the temperature of 25±1°C using three-electrode cell, with Pt mesh counter electrode and reference, saturated calomel electrode (SCE), being placed in separate compartments, while working electrode (Ir covered Ti$_2$AlC) was placed in the main compartment and was connected to the reference electrode through a bridge and a Luggin capillary. All investigated electrodes were first kept in 0.5 M H$_2$SO$_4$ for 10 min at the current density j = -0.1 A cm^{-2} and then polarization curves were recorded starting at -0.016 V and finishing at about -0.14 V with 1 mV s^{-1} (using current interrupt technique). Polarization curves for all samples were also recorded by starting at -0.14 V and finishing at -0.016 V and they were practically the same as those recorded in opposite direction. After recording polarization curves by sweeping potential with 1 mV s^{-1} (using current interrupt technique), EIS measurements were performed at four different potentials (on sample with 22 ML of Ir), covering current density range from approximately -2 mA cm^{-2} to -100 mA cm^{-2}, in the frequency range from 5 kHz to 0.01 Hz, with the amplitude of 5 mV RMS at 20 points per decade.

Since two different reference electrodes were used (SSE and SCE) all potentials in this work are given vs. normal hydrogen electrode (NHE).

3. RESULTS AND DISCUSSION

3.1. Electrodeposition of iridium on Ti₂AlC substrate

As shown in our recent study [31] and explained in the introduction, electrodeposition of iridium could be achieved from x mM K$_3$IrCl$_6$ only in the solution of 0.5 M Na$_2$SO$_4$ (pH 6.2) at the temperature of 70 ^{o}C. Hence, following details given in this work [31], solutions containing 1 and 3 mM K$_3$IrCl$_6$ + 0.5 M Na$_2$SO$_4$ (pH 6.2) were prepared by heating supporting electrolyte to 70 ^{o}C in the main compartment of the cell and adding necessary amount of K$_3$IrCl$_6$ in the supporting electrolyte at 70 ^{o}C. Since it was shown in our previous study [31] that electrodeposition of iridium on Ti$_2$AlC substrate could be achieved only on the reduced Ti$_2$AlC substrate, working electrode was kept at the potential of hydrogen evolution for at least 100 s before recording either LSV or $j - t$ ($Q - t$) responses for iridium electrodeposition.

Samples with 3 ML of Ir and 22 ML of Ir were electrodeposited by LSV (v = 5 mV s^{-1}), Fig. 1a,b, while those with 6 ML of Ir, 10 ML of Ir and 15 ML of Ir were electrodeposited by controlled potential coulometry, Fig. 2 a,b. The reason for application of two techniques for Ir electrodeposition is as follows: the first LSV was recorded in 1 mM K$_3$IrCl$_6$ + 0.5 M Na$_2$SO$_4$ and the amount of electro-deposited Ir was only 3 ML (Fig. 1a); the second LSV was recorded in 3 mM K$_3$IrCl$_6$ + 0.5 M Na$_2$SO$_4$ and the amount of electrodeposited Ir was 22 ML (Fig. 1b); since our intention was to electrodeposit 6, 10 and 15 ML of Ir it was necessary to apply potential controlled coulometry in the solution containing 3 mM K$_3$IrCl$_6$ + 0.5 M Na$_2$SO$_4$ in order to obtain desired amounts of Ir (Fig. 2a,b).

Considering Fig. 1a it could be concluded [31] that the cathodic charge under the LSV peak between -0.2 V and 0.1 V corresponds to the iridium electrodeposition on Ti$_2$AlC substrate, while the cathodic current density at more negative potentials than -0.2 V corresponds to the HER. This charge amounts to approximately 3 ML. With the increase of K$_3$IrCl$_6$ concentration from 1 mM to 3 mM the shape of the LSV changes (Fig. 1b) and under the same conditions the peak current density for iridium electrodeposition increased from ∼ 50 μA cm^{-2} in 1 mM solution to ∼ 670 μA cm^{-2} in 3 mM solution, with the LSV peak being sharper and positioned in the potential range from -0.15 V to 0.15 V. It is interesting to note that before the beginning of iridium electrodeposition, anodic current density (most probably due to desorption of hydrogen) has been recorded.

In the case of controlled potential coulometry the increase of cathodic charge is almost linear (Fig. 2a), while the $j - t$ responses (Fig. 2b) possess practically the same shape.
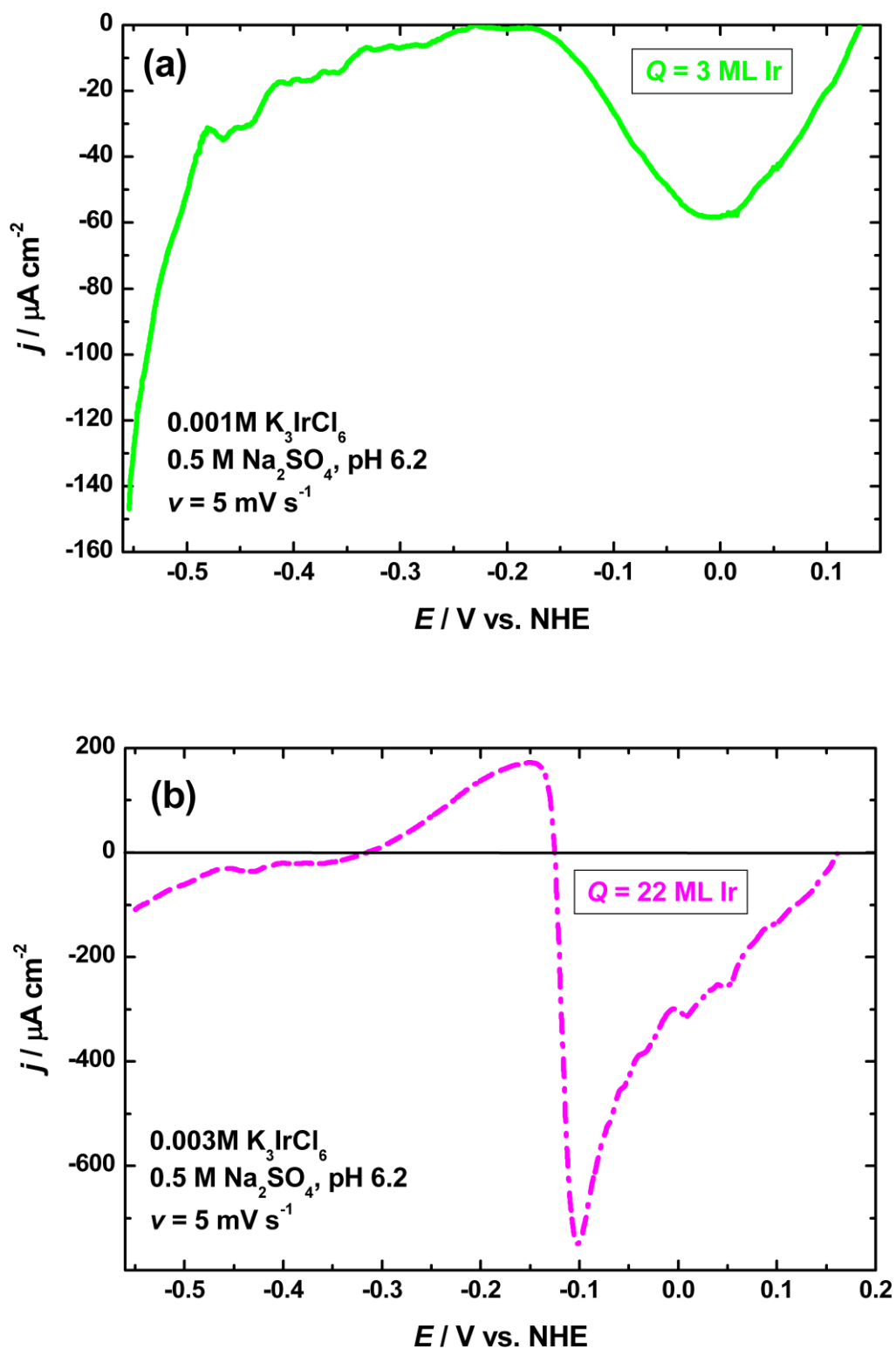
Figure 1. Electrodeposition of samples with 3 ML of Ir (a) and 22 ML of Ir (b) recorded by the LSV with the sweep rate of 5 mV s^{-1}. Solutions: 1 mM and 3 mM K$_3$IrCl$_6$ + 0.5 M Na$_2$SO$_4$ (pH 6.2) at 70 ^{o}C.

Slika 1. Elektrohemijsko taloženje uzoraka sa 3 monosloja Ir (a) i 22 monosloja Ir (b) metodom linerane promene potencijala (v = 5 mV s^{-1}). Rastvori: 1 mM and 3 mM K$_3$IrCl$_6$ + 0.5 M Na$_2$SO$_4$ (pH 6.2), T = 70 ^{o}C.
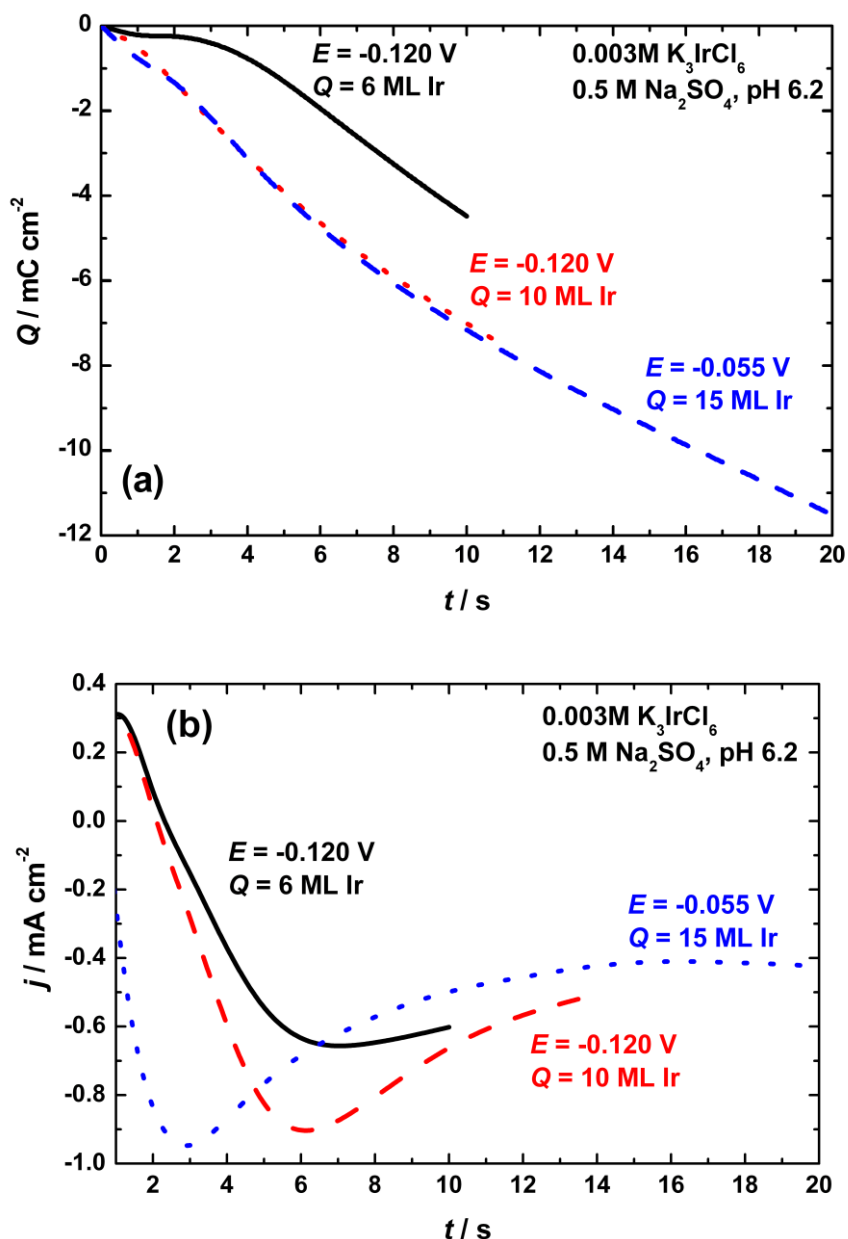
Figure 2. Electrodeposition of samples with 6, 10 and 15 ML of Ir, (a) Q − t, (b) j − t responses recorded with controlled potential coulometry. Solution: 3 mM K₃IrCl₆ + 0.5 M Na₂SO₄ (pH 6.2), T = 70 °C.

Slika 2. Elektrohemijsko taloženje uzoraka sa 6, 10 i 15 monoslojeva pri konstantnom potencijalu do potrebne količine naelektrisanja. Rastvor: 3 mM K₃IrCl₆ + 0.5 M Na₂SO₄ (pH 6.2) at 70 °C.

The amount of charge for close-packed monolayer of iridium was calculated from the equation

$$Q_{ML} = \frac{1}{a}\frac{1}{b} q_e z \qquad (1)$$

where: r – atomic radius of Ir (136 pm, $a = 2r = 272$ pm); b – distance between Ir atoms in two rows of the (111) orientation (235 pm - see Fig. 3); q – charge of one electron (1.602 x 10⁻¹⁹ C); z – number of reduced electrons for Ir electrodeposition (3, $Ir^{3+} \rightarrow Ir^0$). The amount of charge for the formation of one close-packed (111) monolayer of Ir was found to be Q_{ML} = 752 µC cm⁻².
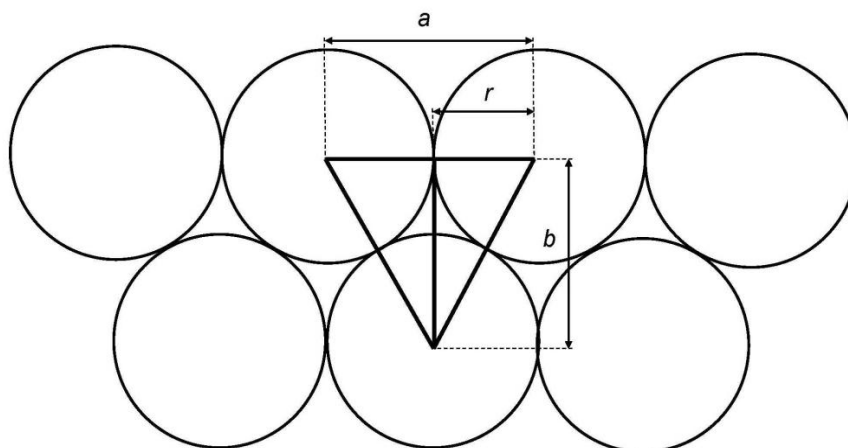
Figure 3. The schematic presentation of the close-packed (111) monolayer of Ir.

Slika 3. Shematski prikaz gusto pakovanog (111) monosloja Ir.

3.2. HER at all investigated samples

Polarization curves for all Ir electrodeposited samples are presented in Fig. 4. As can be seen almost identical polarization curves were obtained for 6, 10, 15 and 22 ML of Ir, while at the sample with 3 ML of Ir the overpotential for the HER starts to increase already at the current density of -100 $\mu A\ cm^{-2}$, indicating that the whole surface of Ti₂AlC substrate is not covered with iridium and that the HER mostly takes place at the substrate surface.

All polarization curves, except that for 3 ML of Ir, are characterized with lower Tafel slope (varying between -14 and -16 mV dec^{-1}) in the range of current densities from about -0.1 mA cm^{-2} to approximately -100 mA cm^{-2} (for the sample with 22 ML of Ir) and the increase of Tafel slope at higher current densities varying between -40 and -72 mV dec^{-1}. These polarization curves are almost identical to those recorded in our previous paper for thicker iridium layers. The overpotential for the HER at samples with 15 and 22 ML of Ir is seen to be very small, amounting to 82 mV only.
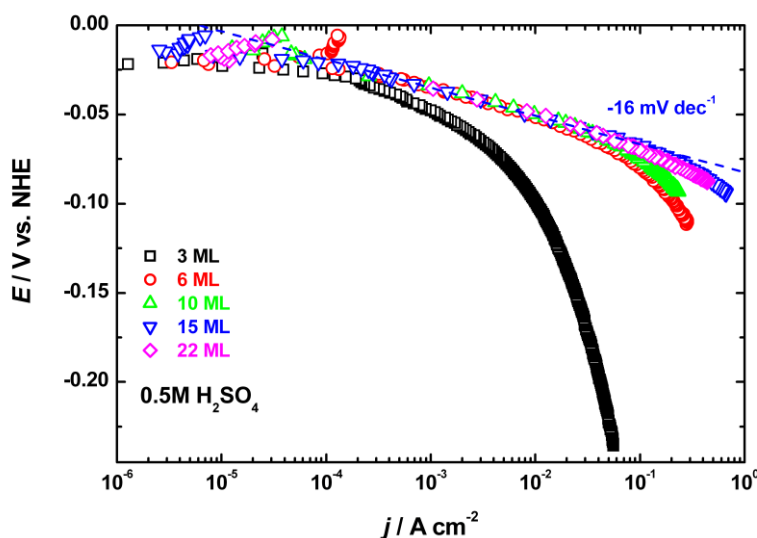

Figure 4. Polarization curves for all electrodeposited Ir samples recorded in 0.5 M H₂SO₄.

Slika 4. Polarizacione krive svih elektrohemijski istaloženih uzoraka Ir u 0.5 M H₂SO₄.

In Fig. 5 is presented the polarization curve for the HER recorded for sample with 6 ML of Ir. From the intercept of Tafel line at lower current densities and zero overpotential, the exchange current density is obtained. Taking into account that the weight of electrodeposited Ir for this sample amounts to 2.995 $\mu g\ cm^{-2}$, high specific exchange current density of -27.89 A g^{-1} is obtained.
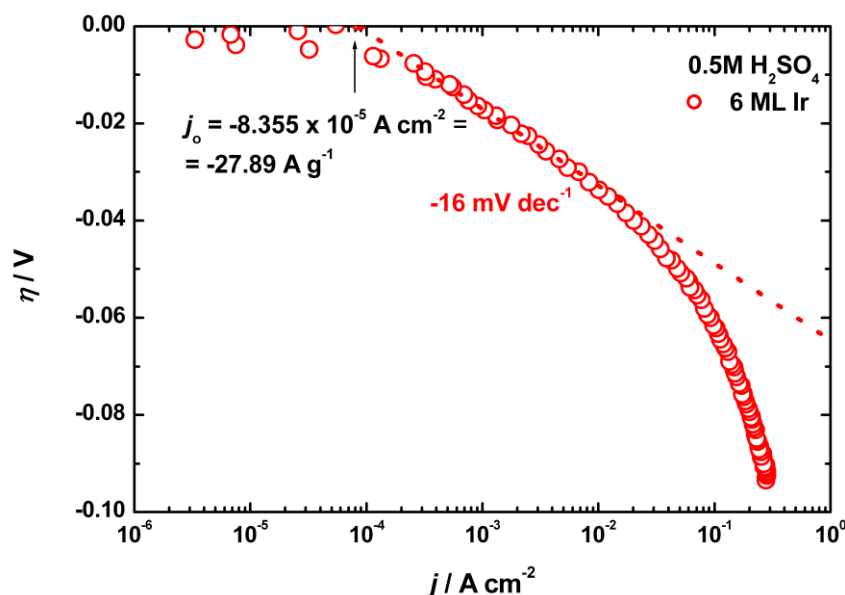
Figure 5. Polarization curve for 6 ML of Ir recorded in 0.5 M H₂SO₄.

Slika 5. Polarizaciona kriva uzorka sa 6 monoslojeva Ir u 0.5 M H₂SO₄.

The theory of the HER on metallic electrodes in acid solutions predicts that this reaction proceeds through a combination of three elementary steps, Volmer step, Heyrovsky step and Tafel step and that hydrogen adsorption takes place under Langmuir conditions. The analysis of Tafel slopes for different cases has been given: If the HER follows the Volmer–Heyrovsky pathway, theoretically two different slopes could be observed on the Tafel plots depending on the rate-determining step (RDS) and surface coverage by H_{ads} (θ_H): only one slope of -120mVdec^{-1} over the entire overpotential range when the Volmer reaction is a RDS, or -40 mV dec^{-1} at lower overpotentials ($\theta_H \rightarrow 0$) and -120 mV dec^{-1} at higher overpotentials ($\theta_H \rightarrow 1$) when the Heyrovsky step is the RDS, while the slope of -30 mV dec^{-1}

implies Tafel step as the rate determining one. Hence, the presence of a Tafel slope of -16 to -18 mV dec^{-1} cannot be explained by a general HER mechanism and formal kinetics laws, but it could be concluded that the HER on such electrodes is very fast, producing high current densities at low overpotentials. There are some hypothesis in the literature that the decrease of Tafel slope values at these catalysts could be caused by significant contribution of the hydrogen oxidation reaction (HOR) to the experimentally recorded HER currents in the low overpotential region [32,33]. Nevertheless, the obtained values of Tafel slopes, as well as exchange current density values in the potential region close to the open circuit potential, represent real behavior of electrodes under these operating conditions [34].
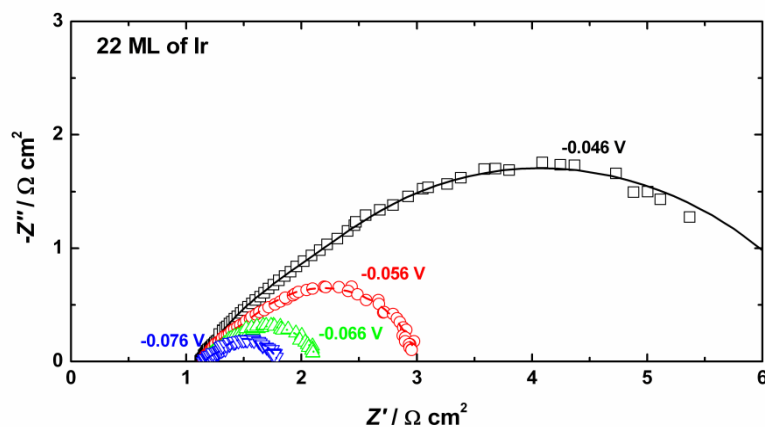

Figure 6. EIS results for sample with 22 ML of Ir recorded in 0.5 M H₂SO₄.

Slika 6. Rezultati merenja impedanse za uzorak sa 22 monosloja Ir u 0.5 M H₂SO₄.

In Fig. 6, EIS results recorded at four different potentials for sample with 22 ML of Ir, are presented. As it could be expected, the semicircles corresponding to the R_{ct} and R_p become smaller with the increase of overpotential for the HER (more negative potentials).
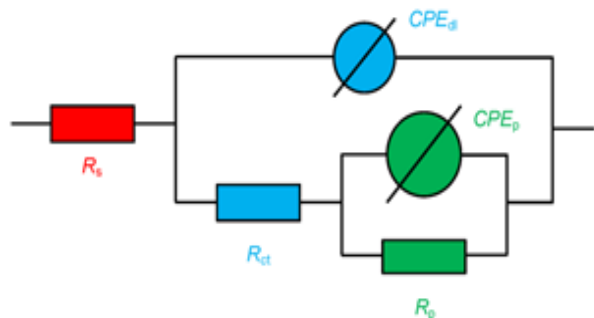

Figure 7. Equivalent circuit for fitting EIS results presented in Figure 6.

Slika 7. Ekvivalentno kolo za fitovanje rezultata impedanse prikazanih na Slici 6.

EIS results (squares, circles, triangles, etc.) were fitted (corresponding lines) with the equivalent circuit typical for the HER reaction [35] presented in Fig. 7. The HER kinetics-related part of this circuit consists of elements $R_p \| CPE_p$ in series with R_{ct}, where parameters R_p and CPE_p are associated with the relaxation of the adsorbed reaction intermediate upon potential perturbation [36], while R_{ct} is the charge transfer resistance. CPE_{dl} is a constant phase element replacing C_{dl}, and R_s is the solution resistance

The values of C_{dl} and C_p were calculated using the equations (2) and (3) [37,38], assuming parallel connection between C_{dl} and R_{ct}, as well as between C_p and R_p

$$C_{dl} = \left[Y_{dl} R_{ct}^{[(\alpha)_{dl}-1]} \right]^{\frac{1}{\alpha_{dl}}} \tag{2}$$

$$C_p = \left[Y_p R_p^{[(\alpha)_p-1]} \right]^{\frac{1}{\alpha_p}} \tag{3}$$

Obtained values for C_{dl} and C_p for sample with 22 ML of Ir, recorded at four different potentials are given in Table 1.

Table 1. Parameters C_{dl} and C_p obtained from Y_{dl} and R_{ct}, Y_p and R_p, using equations (2) and (3).

Tabela 1. Prametri C_{dl} i C_p dobijeni iz Y_{dl} i R_{ct}, Y_p i R_p korišćenjem jednačina (2) i (3).

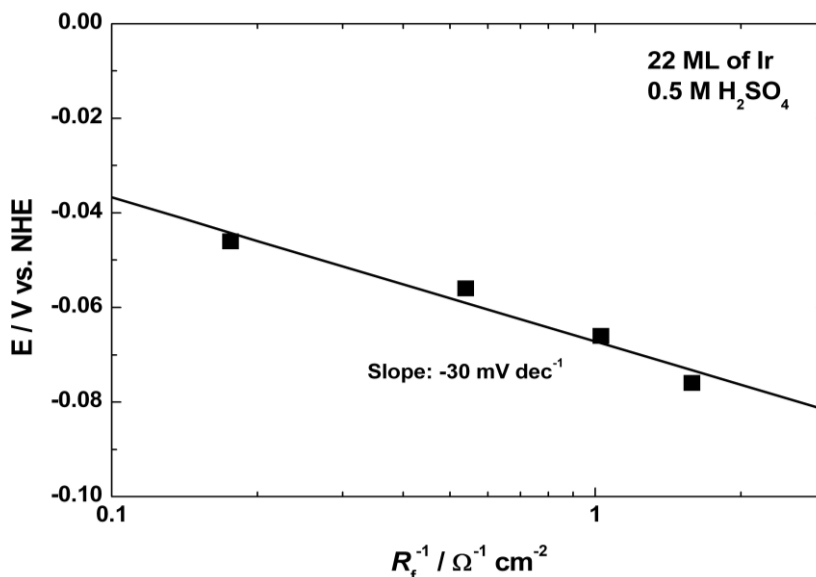| Sample	E / V vs. NHE	C_{dl} / F cm^{-2}	C_p / F cm^{-2}
22 ML of Ir	-0.046	0.032	0.056
	-0.056	0.010	0.048
	-0.066	0.018	0.058
	-0.076	0.013	0.052

Figure 8. E vs. log(R_f^{-1}) dependence obtained by fitting EIS results for sample with 22 ML of Ir recorded in 0.5 M H$_2$SO$_4$.

Slika 8. E vs. log(R_f^{-1}) zavisnost dobijena fitovanjem rezultata imepdanse za uzorak sa 22 monosloja Ir u 0.5 M H$_2$SO$_4$.

Faradaic resistance of the HER, $R_f = R_{ct} + R_p$, was obtained for all samples by fitting EIS results using equivalent circuit presented in Fig. 7. In the case of the HER the dependences E vs. log $(R_f)^{-1}$ should be linear, as it is the case for investigated sample presented in Fig. 8.

4. CONCLUSIONS

It was shown that it is possible to electrdeposit sub-monolayer amounts of Ir (3, 6, 10, 15 and 22 ML) on Ti₂AlC substrate from the solution containing 1mM or 3 mM K_3IrCl_6 + 0.5 M Na_2SO_4 (pH 6.2) at 70 ^{o}C using LSV at a sweep rate of 5 mV s^{-1} and controlled potential coulometry. The HER on Ir-Ti₂AlC samples containing 3, 6, 10, 15 and 22 ML was investigated in 0.5 M H_2SO_4 by recording polarization curves (v = 1 mV s^{-1}), while the EIS at four different potentials has been performed on the sample with 22 ML only. Polarization curves, except the one for 3 ML of Ir, were characterized with the low Tafel slope of -14 to -16 mV dec^{-1} up to about -0.1 A cm^{-2}, while at higher current densities the Tafel slope increased, varying between -40 and -72 mV dec^{-1}. The value of specific exchange current density determined from the polarization curve was the highest for the 6 ML of Ir amounting to -27.89 A g^{-1}. It is important to emphasize excellent catalytic behavior of sub-monolayer Ti₂AlC supported Ir catalysts under industrial conditions of the HER, with the overpotential of 82 mV at j = -0.3 A cm^{-2}. The facts that electrodeposition is considered as a cost effective way for catalyst production, as well as low cost of commercial Ti₂AlC support, make these catalysts promising cathodes for commercial hydrogen production by water electrolysis in sulfuric acid solution.

Acknowledgements

5. REFERENCES

[1] J.Durst, A.Siebel, C.Simon, F.Hasché, J.Herranz, H.A.Gasteiger (2014) New insights into the electrochemical hydrogen oxidation and evolution reaction mechanism, Energy Environ. Sci., 7, 2255−2260.

[2] Y.Pi, N.Zhang, S.Guo, J.Guo, X.Huang (2016) Ultrathin Laminar Ir Superstructure as Highly Efficient Oxygen Evolution Electrocatalyst in Broad pH Range, Nano Lett., 16, 4424-4430.

[3] C.C.L.McCrory, S.Jung, J.C.Peters, T.F.Jaramillo (2013) Benchmarking Heterogeneous Electrocatalysts for the Oxygen Evolution Reaction, J. Am. Chem. Soc., 135, 16977-16987.

[4] P.Lettenmeier, L.Wang, U.Golla-Schindler, P. Gazdzicki, N.A.Canas, M.Handl, R.Hiesgen, S.S.Hosseiny, A.S. Gago, K.A.Friedrich (2016) Nanosized IrOx–Ir Catalyst with Relevant Activity for Anodes of Proton Exchange Membrane Electrolysis Produced by a Cost-Effective Procedure, Angew. Chem.,128, 752-756.

[5] L.C.Seitz, C.F.Dickens, K.Nishio, Y.Hikita, J. Montoya, A.Doyle, C.Kirk, A.Vojvodic, H.Y.Hwang, J.K.Norskov, T.F.Jaramillo (2016) A highly active and stable IrOx/SrIrO3 catalyst for the oxygen evolution reaction, Science, 2016, 353, 1011-1014.

[6] P.-Y.Liu, C.-C.Hsu, M.-C.Chuang (2017) Hemin-mediated construction of iridium oxide with superior stability for the oxygen evolution reaction, J. Mater. Chem. A, 5, 2959-2971.

[7] H.-S.Oh, H.N.Nong, T.Reier, A.Bergmann, M. Gliech, J.F.deAraujo, E.Willinger, R.Schlogl, D.Teschner, P.Strasser (2016) Electrochemical Catalyst–Support Effects and Their Stabilizing Role for IrO$_x$ Nanoparticle Catalysts during the Oxygen Evolution Reaction, J. Am. Chem. Soc., 138, 12552-12563.

[8] D.F.Abbott, D.Lebedev, K.Waltar, M.Povia, M.Nachtegaal, E.Fabbri, C.Coperet, T.J.Schmidt (2016) Iridium Oxide for the Oxygen Evolution Reaction: Correlation between Particle Size, Morphology, and the Surface Hydroxo Layer from Operando XAS, Chem. Mater., 28, 6591-6604.

[9] P.Jiang, J.Chen, C.Wang, K.Yang, S.Gong, S.Liu, Z.Lin, M.Li, G.Xia, Y.Yang, J.Su, Q.Chen (2018) Tuning the Activity of Carbon for Electrocatalytic Hydrogen Evolution via an Iridium-Cobalt Alloy Core Encapsulated in Nitrogen-Doped Carbon, Cages. Adv. Mater., 30(9), 1705324.

[10] K.A.Kuttiyiel, K.Sasaki, W.-F.Chen, D.Sub, R.R.Adzic (2014) Core–shell, hollow-structured iridium–nickel, J. Mater. Chem. A, 2, 591-594.

[11] Y.Pi, Q.Shao, P.Wang, J.Guo, X.Huang (2017) General Formation of Monodisperse IrM (M = Ni, Co, Fe) Bimetallic Nanoclusters as Bifunctional Electrocatalysts for Acidic Overall Water Splitting, Adv. Funct. Mater., 27, 1700886. https://doi.org/10.1002/adfm.201700886

[12] J.Feng, F.Lv, W.Zhang, P.Li, K.Wang, C.Yang, B. Wang, Y.Yang, J.Zhou, F.Lin, G.C.Wang, S.Guo (2017) Iridium-Based Multimetallic Porous Hollow Nanocrystals for Efficient Overall-Water-Splitting Catalysis, Adv. Mater., 29, 1703798.

[13] L.Fu, G.Cheng, W.Luo (2017) Colloidal synthesis of monodisperse trimetallic IrNiFe nanoparticles as highly active bifunctional electrocatalysts for acidic overall water splitting, J. Mater. Chem. A, 5, 24836–24841.

[14] J.Zhang, G.Wang, Z.Liao, P.Zhang, F.Wang, X. Zhuang, E.Zschech, X.Feng (2017) Iridium nano-particles anchored on 3D graphite foam as a bifu-nctional electrocatalyst for excellent overall water splitting in acidic solution, Nano Energy, 40, 27–33.

[15] L.Fu, X.Zeng, G.Cheng, W.Luo (2018) IrCo Nanodendrite as an Efficient Bifunctional Electrocatalyst for Overall Water Splitting under Acidic Conditions, ACS Appl. Mater. Interfaces, 10, 24993−24998.

[16] J.Mahmood, M.A.R.Anjum, S.H.Shin, I.Ahmad, H.J.Noh, S.J.Kim, H.Y.Jeong, J.S.Lee, J.B.Baek (2018) Encapsulating Iridium Nanoparticles Inside a 3D Cage-Like Organic Network as an Efficient and Durable Catalyst for the Hydrogen Evolution Reaction, Adv. Mater., 1805606.

[17] L.Fu, F.Yang, G.Cheng, W.Luo (2018) Ultrathin Ir nanowires as high-performance electrocatalysts for efficient water splitting in acidic media, Nanoscale, 10, 1892-1897.

[18] J. Hämäläinen, M. Ritala, M. Leskelä (2014) Atomic Layer Deposition of Noble Metals and Their Oxides, Chem. Mater., 26, 786-801.

[19] Y. Liu, D. Gokcen, U. Bertocci, T.P. Moffat (2012) Self-Terminating Growth of Platinum Films by Electrochemical Deposition, Science, 338,1327-1330.

[20] Y. Liu, C.M. Hangarter, D. Garcia, T.P. Moffat (2015) Self-terminating electrodeposition of ultrathin Pt films on Ni: An active, low-cost electrode for H2 production, Surf. Sci., 631,141-154.

[21] S.H.Ahn, H.Tan, M.Haensch, Y.Liu, L.A.Bendersky, T.P.Moffat (2015) Self-terminated electrodeposition of iridium electrocatalysts, Energy Environ. Sci., 8, 3557-3562.

[22] E.L.Macnamara (1962) The Electrodeposition of Iridium, J. Electrochem. Soc., 109, 61–63.

[23] T.Ohsaka, M.Isaka, K.Hirano, T.Ohishi (2008) Effect of ultrasound sonication on electroplating of iridium, Ultrason. Sonochem., 15, 283–288.

[24] G.Sheela, M.Pushpavanam, S.Pushpavanam (1999) Electrodeposition of iridium, B. Electrochem., 15, 208–210.

[25] E.N.El Sawy, V.I.Birss (2009) Nano-porous iridium and iridium oxide thin films formed by high efficiency electrodeposition J. Mater. Chem., 19, 8244–8252.

[26] A.Cusanelli, U.Frey, D.T.Richens, A.E.Merbach (1996) The Slowest Water Exchange at a Homoleptic Mononuclear Metal Center: Variable-Temperature and Variable-Pressure 17O NMR Study on [Ir(H$_2$O)$_6$]$^{3+}$, J. Am. Chem. Soc., 118, 5265-5271.

[27] S.Dong, C.Wu, K.Li, Z.Chai, X.Mao, X.Dai (2000) Coulometric titration study of the redox behavior and precise determination of hexachloroiridate(IV) ion and its monoaquo-chloro complex with electrogenerated bi-intermediates, Anal. Chim. Acta, 415, 185-191.

[28] J.C.Chang, C.S.Garner (1965) Kinetics of Aquation of Aquopentachloroiridate(III) and Chloride Anation of Diaquotetrachloroiridate(III) Anions, Inorg. Chem., 4, 209-215.

[29] B.M.Jović, V.D.Jović, U.Č.Lačnjevac, S.Stevanović, M.Radović, N.V.Krstajić (2016) Ru layers electrodeposited onto highly stable Ti$_2$AlC substrates as cathodes for hydrogen evolution in sulfuric acid solutions, J. Electroanal. Chem., 766, 78–86.

[30] B.M.Jović, V.D.Jović, G.Branković, M.Radović, N.V.Krstajić (2017) Hydrogen evolution in acid solution at Pd electrodeposited onto Ti$_2$AlC, Electrochim. Acta, 224 (2017) 571–584.

[31] N.Elezović, G.Branković, P.Zabinski, M.Marzec, VD.Jović (2020) Ultra-thin layers of iridium electrodeposited on Ti$_2$AlC substrate as efficient catalysts for hydrogen evolution in acid solutions, Accepted for publication in J. Electroanal. Chem.

[32] J.Zheng, Y.Yan, B.Xu (2015) Correcting the Hydrogen Diffusion Limitation in Rotating Disk Electrode Measurements of Hydrogen Evolution Reaction Kinetics, J. Electrochem. Soc., 162, F1470-F1481.

[33] W.Sheng, H. A.Gasteiger, Y.Shao-Horn (2010) Hydrogen Oxidation and Evolution Reaction Kinetics on Platinum: Acid vs Alkaline Electrolytes, J. Electrochem. Soc., 157, B1529-B1536.

[34] U.Lačnjevac, R.Vasilić, T.Tokarski, G.Cios, P.Zabiński, N.Elezović, N.Krstajić (2018) Deposition of Pd nanoparticles on the walls of cathodically hydrogenated TiO$_2$ nanotube arrays via galvanic displacement: A novel route to produce exceptionally active and durable composite electrocatalysts for cost effective hydrogen evolution, Nano Energy, 47, 527–538.

[35] R.D.Armstrong, M.Henderson (1972) Impedance plane display of a reaction with an adsorbed intermediate, J. Electroanal. Chem., 39, 81-90.

[36] D.A.Harrington, B.E.Conway (1987) AC impedance of faradaic reactions involving electrosorbed intermediates–I. Kinetic theory, Electrochim. Acta, 32, 1703-1712.

[37] V.D.Jovic (2015) Determination of the correct value of C_{dl} from the impedance results fitted by the commercially available software, http://www.gamry.com

[38] M.E.Orazem, P.Shukla, M.A.Membrino (2002) Extension of the measurement model approach for deconvolution of underlying distributions for impedance measurements, Electrochim. Acta, 47, 2027-2034.

IZVOD

NEKOLIKO MONOSLOJEVA ELEKTROHEMIJSKI ISTALOŽENOG IRIDIJUMA NA PODLOZI OD Ti₂AlC KAO KATALIZATORI ZA IZDVAJANJE VODONIKA U RASTVORU SUMPORNE KISELINE

Izdvajanje vodonika ispitivano je u rastvoru sumporne kiseline na elektrohemijski istaloženim slojevima (od 3 monosloja do 22 monosloja) iridijuma na podlozi od Ti₂AlC. Najmanja i najveća količina iridijuma (3 i 22 monosloja) elektrohemijski su istaložene metodom linearne voltametrije, dok su preostala tri uzorka (6, 10 i 15 monoslojeva) elektrohemijski istaložena pri konstantnom potencijalu do potrebne količine naelektrisanja iz rastvora 1 mM, ili 3 mM K_3IrCl_6 + 0.5 M Na_2SO_4 (pH 6.2) na temperaturi rastvora od 70 ^oC. Reakcija izdvajanja vodonika ispitivana je na svim elektrodama snimanjem polarizacionih krivih. Za uzorak sa 22 monosloja Ir primenjena je i metoda impedanse. Polarizacione krive za uzorke sa 6, 10, 15 i 22 monosloja Ir bile su okarakterisane malom vrednošću Tafel-ovog nagiba od -14 to -16 mV dek^{-1} u oblasti gustina struja do -0.1 A cm^{-2}, dok se Tafel-ov nagib povećavao pri većim gustinama struja varirajući od -40 do -72 mV dek^{-1}. Najveća vrednost specifične gustine struje izmene (j_o) dobijena je kod uzorka sa 6 monoslojeva Ir i iznosila je - 27.89 A g^{-1}. Za uzorke sa 15 i 22 monosloja Ir vrednost prenapetosti pri gustini struje j = -0.3 A cm^{-2} (uslovi industrijske proizvodnje vodonika) iznosila je 82 mV.

Ključne reči: *izdvajanje vodonika, elektrohemijsko taloženje Ir (3 do 22 monosloja), sumporna kiselina.*